Sciencexpress Report

Explaining the Structure of the Archean Mass-Independent Sulfur Isotope Record

Itay Halevy,* David T. Johnston, Daniel P. Schrag

Department of Earth and Planetary Sciences, Harvard University, Cambridge, MA USA.

*To whom correspondence should be addressed. E-mail: itay.halevy@gmail.com

Sulfur isotopes in ancient sediments provide a record of past environmental conditions. The long-timescale variability and apparent asymmetry in the magnitude of minor sulfur isotope fractionation in Archean sediments remain unexplained. Using an integrated biogeochemical model of the Archean sulfur cycle, we find that the preservation of mass-independent sulfur is influenced by a variety of extra-atmospheric mechanisms including biological activity and continental crust formation. Preservation of atmospherically produced mass-independent sulfur implies limited metabolic sulfur cycling prior to ~2500 Ma; the asymmetry in the record requires that bacterial sulfate reduction was geochemically unimportant at this time. Our results suggest that the large-scale structure of the record reflects variability in the oxidation state of volcanic sulfur volatiles.

Most natural processes fractionate sulfur in proportion to the mass difference between the isotopes (*1*). Ultraviolet photolysis of atmospheric SO_2, however, produces a mass-independent fractionation (MIF), which is delivered to the surface only if atmospheric O_2 levels are very low (*2–7*). The presence of MIF in sedimentary sulfides and sulfates older than 2450 Ma, and its absence from later sediments has led to the accepted view that atmospheric O_2 levels crossed a threshold value near the Archean–Proterozoic boundary (*2–6*). Beyond simply recording MIF, the Archean sulfur isotope record appears to carry a discernable temporal structure: moderate (<4‰) early Archean $\Delta^{33}S$ anomalies followed by a mid-Archean minimum (<2‰), and a late Archean explosion in the magnitude of MIF (<12‰ in $\Delta^{33}S$). Previous studies attribute this variability to changes in the composition and oxidation state of the atmosphere, and the associated evolution of photochemical pathways (*7–9*). In addition, an asymmetry in the record, with strongly positive but only weakly negative isotopic anomalies, remains without a quantitative explanation.

Here we explore the effect of a variety of extra-atmospheric processes on the characteristics and preservation of MIF. We present an integrated model of the full surface sulfur cycle, accounting for the production and translation of atmospherically derived MIF through a marine reservoir and its preservation in the geologic record (*10*). We use recent measurements and theoretical calculations of $^{3x}SO_2$ (x = 2,3,4,6) UV absorption cross-sections to constrain atmospheric MIF production (*10–12*). Solving mass-balance equations for the steady state reservoir sizes and isotopic compositions of four different oxidation states of sulfur: S^{6+} (sulfate), S^{4+} (sulfite, SO_2), S^0 (elemental sulfur), and S^{2-} (sulfide, H_2S), we track MIF from production to lithification.

Rates of volcanic supply, photolytic destruction, gas-phase reactions and net deposition to the surface govern the atmospheric lifetime of SO_2. Any process that destroys atmospheric SO_2 at the expense of photolysis reduces the production, by mass, of MIF (e.g., atmospheric oxidation, Fig. 1A), but as long as photolysis rates are non-negligible relative to the other atmospheric SO_2 sinks, MIF is produced (though not necessarily preserved). In addition to non-photolytic atmospheric sinks, which attenuate MIF by decreasing production, homogenization reduces MIF by remixing anomalous compositions back toward the original SO_2 value. Whereas atmospheric oxidation to sulfate has been discussed in this context (*6*), microbial processes, which can perform a similar function, have not been rigorously investigated (Fig. 1B). Given a quantitatively significant flux of MIF from SO_2 photolysis, cycling between the sulfur reservoirs (e.g., microbial activity) or transformation to one oxidation state (e.g., quantitative reduction to sulfide) must be minor, as not to erase the anomaly. An immediate implication is that low atmospheric O_2 is necessary but insufficient for preservation of MIF in the geologic record.

Our model results illustrate the sensitivity of MIF to a few key properties of the ocean-atmosphere system, and its relative insensitivity to several others. Atmospheric deposition of SO_2 leads to its speciation in seawater $\left[SO_2(aq) \rightleftharpoons HSO_3^- + H^+ \rightleftharpoons SO_3^{2-} + H^+\right]$, where subsequent oxidation by Fe^{3+} (*13–15*) leaves other aqueous oxidation pathways less important (e.g., Fe^{2+}-catalyzed oxidation by aqueous O_2 or by atmospherically produced H_2O_2). This leaves vanishingly little marine S^{4+} (~10^{-3} μM), and only modest sulfate concentrations (~10^2 μM). Given these oxidation rates, the absolute magnitude of MIF is only moderately sensitive to the adopted rate of S^{4+}

disproportionation (Fig. 1D) (*10*), although the symmetry of the sulfate–elemental sulfur MIF is rate sensitive. This is because the isotopic composition of SO_2 propagates to both sulfate and elemental sulfur when disproportionation is rapid, but only to sulfate when oxidation dominates. The asymmetry of the MIF record (Fig. 3) suggests that oxidation, not disproportionation, was the dominant aqueous S^{4+} sink. Hydrated formaldehyde complexes S^{4+}, preventing its oxidation and disproportionation; however, this only affects MIF preservation at concentrations higher than those likely in an Archean ocean (Fig. 1E) (*16*).

The magnitude of MIF in pyrite, but not in sulfates, is very sensitive to the SO_2:H_2S ratio in volcanic volatiles (Fig. 1C). This is because the elemental sulfur that ends up in pyrite originates from both atmospheric SO_2 and H_2S, but H_2S photoreactions do not generate MIF. When the outgassing rate of SO_2 increases relative to that of H_2S, more of the elemental sulfur budget comes from SO_2 photolysis and, as a result, is anomalously fractionated. Sulfate, on the other hand, is produced almost entirely from oxidation and photolysis of SO_2, and so its isotopic composition is insensitive to changes in the relative abundance of SO_2 and H_2S. Changes in the total sulfur ($SO_2 + H_2S$) outgassing rate with constant SO_2:H_2S produce no change in MIF magnitudes (Fig. 1F), but this may be due to the simplified nature of our atmospheric model; S_8 production in more detailed atmospheric models is sensitive to the total sulfur outgassing rate (*7*, *17*). We note, however, that more rapid S_8 production does not necessarily translate into stronger MIF if the S_8 is H_2S-derived.

MIF depends critically on the partial pressure of CO_2 (pCO_2); increased pCO_2 results in stronger scattering and UV absorption, decreasing SO_2 photolysis rates (Fig. 2A), and in more detailed atmospheric models, the relative abundances of atmospheric CO_2 and CH_4 also influence SO_2 oxidation rates and the efficacy of MIF export (*6*, *7*, *17*). Our model highlights that with a more acidic ocean (at high pCO_2) the degree of pyrite saturation decreases, and H_2S partitions more strongly into the atmosphere. As the importance of H_2S photolysis relative to pyrite precipitation increases, more S^0 is H_2S-derived. This does not affect the $\Delta^{33}S$ of sulfate ($\Delta^{33}S_{sulfate}$) but decreases the $\Delta^{33}S$ of pyrite ($\Delta^{33}S_{pyr}$; Fig. 2B, dotted lines) and influences the symmetry of the $\Delta^{33}S$ signal.

Four properties emerge as important for the preserved magnitude and symmetry of Archean MIF: atmospheric SO_2 oxidation rates, redox transformations (including microbial cycling rates), SO_2:H_2S in volcanic gases, and pCO_2. The very presence of MIF in the rock record points to low oxidant availability, suggesting that atmospheric oxidation was not the dominant SO_2 sink (*6*, *7*). With constraints from the geologic record on the remaining three properties, we explore their potential to explain the structure in the Archean MIF record using two quantities: $\Delta^{33}S_{pyr}$ and R_{asym}, a measure of the absolute asymmetry $\left(\left|\Delta^{33}S_{pyr} / \Delta^{33}S_{sulfate}\right|\right)$. A successful explanation of the record must account for early Archean $\Delta^{33}S_{pyr} \approx 4‰$ and $R_{asym} \approx 2$, mid-Archean $\Delta^{33}S_{pyr} \approx 2‰$ and $R_{asym} \approx 1$, and latest Archean $\Delta^{33}S_{pyr} \approx 11‰$ and $R_{asym} > 5$.

When imposed on a purely abiological early Archean sulfur cycle, metabolic cycling between the different sulfur pools can potentially explain portions of the Archean MIF record (Fig. 1B). Both microbial S^0 disproportionation and dissimilatory sulfate reduction may have existed since ~3500 Ma (*18*, *19*). Adopting for the moment a scenario in which biological sulfur cycling is not important prior to ~3500 Ma, an increase in the role of microorganisms equivalent to ~10% modern cycling rates could drive a change in $\Delta^{33}S_{pyr}$ and R_{asym} similar to that observed from the early to mid-Archean (Fig. 3B, *i*→*ii*′). Difficulty arises, however, when microorganisms persist into the late Archean. Given that sulfate reduction delivers $\Delta^{33}S < 0$ to sulfide, a greater degree of symmetry (and even reversed asymmetry, $R_{asym} < 1$) would be expected for the late Archean; this is a marked contrast from the observed R_{asym} of 5–6 and suggests that dissimilatory sulfate reduction only rises to geochemical significance between 2400 and 2500 Ma, when high MIF magnitudes and large asymmetry are no longer observed. A late Archean or early Paleoproterozoic onset of sulfate reduction is consistent with a reanalysis of $\delta^{34}S$ records (*10*), and suggests an explanation for the persistence of nonzero and relatively symmetric MIF for 10 to 100 Myr post-dating the major loss of MIF at ~2500 Ma in some locations (*5*), but not in others (*20*).

In the absence of biological sulfur cycling, we find that with constant volcanic SO_2:H_2S, climatically reasonable changes in pCO_2 (*21*–*23*) cannot alone produce the observed MIF history (Fig. 3A). If we adopt instead an evolving value for Archean pCO_2, calculated to offset changes in solar luminosity and to maintain liquid water [together with ~10 ppmv atmospheric methane maintained by about twice modern seafloor serpentinization rates; (*21*–*24*)], changes in volcanic SO_2:H_2S well within observed values (*25*, *26*) easily account for the histories of both $\Delta^{33}S_{pyr}$ and R_{asym} (Fig. 3A, *i*→*ii*→*iii*). This result does not preclude further changes in pCO_2 affecting the MIF signal [e.g., through the effect of methanogens on pCO_2 and pCH_4 (*21*, *23*)], though the asymmetry in the latest Archean almost by necessity indicates a significant increase in volcanic SO_2:H_2S. Such an increase may be related to a major shift in the style of large igneous province eruption from submarine to subaerial in the late Archean (2700 to 2500 Ma), also suggested to have been the cause for the rise in atmospheric O_2 and the loss of MIF (*25*). Consistent with the sulfur isotope record, our results suggest that this loss would be preceded by a MIF spike due to the elevated volcanic SO_2:H_2S. A small clustering of plume

events during the early Archean [3500 to 3300 Ma (*27*)] may suggest an attendant increase in SO_2:H_2S, explaining the earliest MIF record, though it is not clear that these events were subaerial. The eruption rate required to raise global volcanic SO_2:H_2S from ~1.5 to ~8 (as in Fig. 3A, *ii*→*iii*) is only about half to twice that of the Hawaiian plume (*28*), if the magma composition and SO_2:H_2S are comparable to those of Hawaii [1000 to 1500 ppm sulfur, SO_2:H_2S of 50 to 100 (*26*)]. Given the plausibility of these changes, the structure of the $\Delta^{33}S$ record may speak to large-scale crustal processes, superimposed onto and participating with low-O_2 atmospheric chemistry.

Despite oceanic anoxia, rapid oxidation of SO_2 by Fe^{3+} in the surface ocean suggests that, like the present, deposition into the Archean ocean was a terminal sink for atmospheric SO_2 with a characteristic timescale of a few days. This implies that atmospheric SO_2 was not well mixed and that spatio-temporal variability in its concentration is expected. Considering the demonstrated sensitivity of MIF to the relative abundance of SO_2, this translates into the potential for large variability in pyrite $\Delta^{33}S$, with a much more muted signal in the $\Delta^{33}S$ of sulfate minerals (Fig. 3). Additional variability in pyrite $\Delta^{33}S$ is expected as a result of small-scale processes occurring in sediment pore water, given the possibility for sedimentary sulfides to adopt MIF from a variety of sources [dissolved sulfide, elemental sulfur, sulfite or sulfate (*17*, *29*)]. An aqueous oxidation origin for most of the oceanic sulfate may also explain the lack of correlation between $\Delta^{17}O$ and $\Delta^{33}S$ in early Archean barite (*30*).

Changes in atmospheric composition and chemistry likely explain a fraction of the variability in the Archean MIF record. In addition, we highlight the importance of variability in volcanic SO_2:H_2S, which may have caused the spike in MIF magnitudes around 2700 Ma, immediately preceding the ultimate loss of MIF brought about by the rise of atmospheric O_2. In the absence of atmospheric O_2 and a complex biosphere, it may have been the interactions between the solid Earth (mantle-crust) and fluid Earth (ocean-atmosphere) that drove the sedimentary record of $\Delta^{33}S$.

References and Notes

1. J. R. Hulston, H. G. Thode, *J. Geophys. Res.* **70**, 3475 (1965).
2. MIF is expressed as the difference in per mil (‰) between measured isotopic compositions and those expected if the fractionations were mass-dependent: $\Delta^{33}S \equiv \delta^{33}S - 0.515 \times \delta^{34}S$, $\Delta^{36}S \equiv \delta^{36}S - 1.89 \times \delta^{34}S$.
3. J. Farquhar, J. Savarino, S. Airieau, M. H. Thiemens, *J. Geophys. Res. Planets* **106**, 32829 (2001).
4. J. Farquhar, H. M. Bao, M. Thiemens, *Science* **289**, 756 (2000).
5. J. Farquhar, B. A. Wing, *Earth Planet. Sci. Lett.* **213**, 1 (2003).
6. A. A. Pavlov, J. F. Kasting, *Astrobiology* **2**, 27 (2002).
7. K. Zahnle, M. Claire, D. Catling, *Geobiology* **4**, 271 (2006).
8. S. D. Domagal-Goldman, J. F. Kasting, D. T. Johnston, J. Farquhar, *Earth Planet. Sci. Let.t* **269**, 29 (2008).
9. J. Farquhar *et al*., *Nature* **449**, 706 (2007).
10. Further details are in the supporting online material.
11. S. O. Danielache, C. Eskebjerg, M. S. Johnson, Y. Ueno, N. Yoshida, *J. Geophys. Res. Atmos.* **113**, (2008).
12. H. Ran, D. Q. Xie, H. Guo, *Chem. Phys. Lett.* **439**, 280 (2007).
13. Photo-oxidation of Fe^{2+} (*14*), thought to have been abundant in the Archean ocean (*15*), exceeds SO_2 deposition under most circumstances (*10*).
14. P. S. Braterman, A. G. Cairns-Smith, R. W. Sloper, *Nature* **303**, 163 (1983).
15. H. D. Holland, in *Treatise on Geochemistry* **6**, 583 (2004).
16. H. J. Cleaves II, *Precamb. Res.* **164**, 111 (2008).
17. S. Ono *et al*., *Earth Planet. Sci. Lett.* **213**, 15 (2003).
18. P. Philippot *et al*., *Science* **317**, 1534 (2007).
19. Y. A. Shen, R. Buick, D. E. Canfield, *Nature* **410**, 77 (2001).
20. Q. Guo *et al*., *Geology* **37**, 399 (2009).
21. J. D. Haqq-Misra, S. D. Domagal-Goldman, P. J. Kasting, J. F. Kasting, *Astrobiology* **8**, 1127 (2008).
22. P. Von Paris *et al*., *Planet. Space Sci.* **56**, 1244 (2008).
23. A. A. Pavlov, J. F. Kasting, L. L. Brown, K. A. Rages, R. Freedman, *J. Geophys. Res. Planets* **105**, 11981 (2000).
24. S. Emmanuel, J. J. Ague, *Geophys. Res. Lett.* **34**, (2007).
25. L. R. Kump, M. E. Barley, *Nature* **448**, 1033 (2007).
26. M. M. Halmer, H.-U. Schmincke, H.-F. Graf, *J. Volcanol. Geotherm. Res.* **115**, 511 (2002).
27. A. E. Isley, D. H. Abbott, *J. Geophys. Res. Solid Earth* **104**, 15461 (1999).
28. E. Van Ark, J. Lin, *J. Geophys. Res. Solid Earth* **109**, 11401 (2004).
29. J. R. Lyons, *Chem. Geol.* **267**, 164 (2009).
30. H. M. Bao, D. Rumble, D. R. Lowe, *Geochim. Cosmochim. Acta* **71**, 4868 (2007).

31. I.H. was supported by the Harvard University Origins of Life Initiative, and D.T.J. by NASA Exobiology. D.P.S. thanks support from H. Breck and W. Breck. We thank three anonymous reviewers.

Supporting Online Material

www.sciencemag.org/cgi/content/full/science.1190298/DC1
SOM Text
Figs. S1 to S3
Tables S1 and S2
References

31 March 2010; accepted 17 May 2010
Published online 27 May 2010; 10.1126/science.1190298
Include this information when citing this paper.

Fig. 1. The sensitivity of MIF in pyrite and sulfate, for pCO_2 of 0.01 and 0.1 atm, plotted as a function of (**A**) the fraction of outgassed SO_2 that is oxidized in the atmosphere, (**B**) microbial cycling, represented as a multiple of the sum of nonbiological sinks, (**C**) SO_2:H_2S in volcanic gases, (**D**) the disproportionation rate constant, (**E**) the hydrated formaldehyde concentration, and (**F**) the total sulfur (SO_2 + H_2S) outgassing rate. Metabolisms included in (C) are sulfate reduction, elemental sulfur oxidation, disproportionation and reduction, and sulfide oxidation. Also shown are estimates of modern biological sulfur cycling, and volcanic outgassing.

Fig. 2. The sensitivity of (**A**) the SO_2 column photolysis rate, and (**B**) MIF in pyrite (black) and in sulfates (gray) to pCO_2. Dashed lines represent the response of MIF to changes in atmospheric opacity due to increased molecular absorption and scattering by CO_2, with pCO_2 held constant at 0.01 atm in the ocean. Dotted lines represent the response to changes in the ocean (pH, Fe^{3+} concentration, etc.), with pCO_2 held constant at 0.01 atm in the atmosphere. Solid lines show the combined effect.

Fig. 3. The dependence of preserved MIF on pCO_2, volcanic SO_2:H_2S, and biological activity. (**A**) Color contours of pyrite $\Delta^{33}S$ ($\Delta^{33}S_{pyr}$) with no biological sulfur cycling, highlighting values relevant to the early, middle and late Archean (solid black lines). Also shown are contours of the absolute value of the ratio of pyrite to sulfate $\Delta^{33}S$ (R_{asym}, dotted white lines). (**B**) Same as (A), but with biological cycling between sulfate, sulfur and sulfide at ~10% modern values. (**C**) A section (*i*→*ii*→*iii*) through the phase space plotted in (A), with gradually evolving pCO_2 (red line), and the value of volcanic SO_2:H_2S required to reproduce the observed $\Delta^{33}S_{pyr}$ and R_{asym} (thick gray line). The modeled $\Delta^{33}S$ of pyrite (thick solid black line) and sulfate minerals (thick dashed black line) is compared with the observed record (gray circles) in the lower half of (C). Regions *iii′* in (A) and *ii′* in (B) illustrate the effect on pCO_2 of biological methanogenesis, and on $\Delta^{33}S_{pyr}$ of microbial sulfur cycling, respectively.

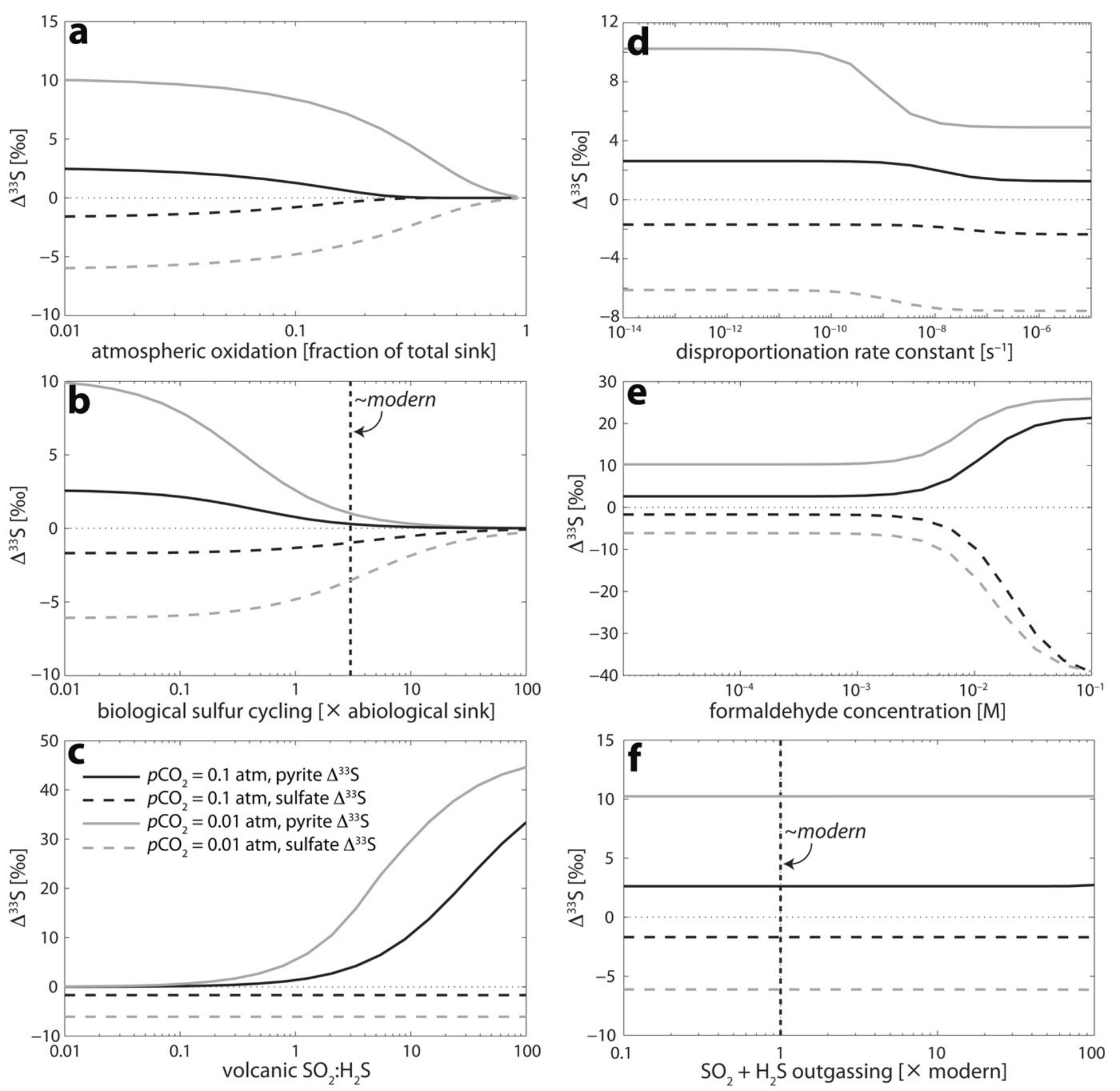
a
Δ33S [‰]
atmospheric oxidation [fraction of total sink]
b
~modern
biological sulfur cycling [× abiological sink]
c
pCO2 = 0.1 atm, pyrite Δ33S
pCO2 = 0.1 atm, sulfate Δ33S
pCO2 = 0.01 atm, pyrite Δ33S
pCO2 = 0.01 atm, sulfate Δ33S
volcanic SO2:H2S
d
disproportionation rate constant [s−1]
e
formaldehyde concentration [M]
f
~modern
SO2 + H2S outgassing [× modern]

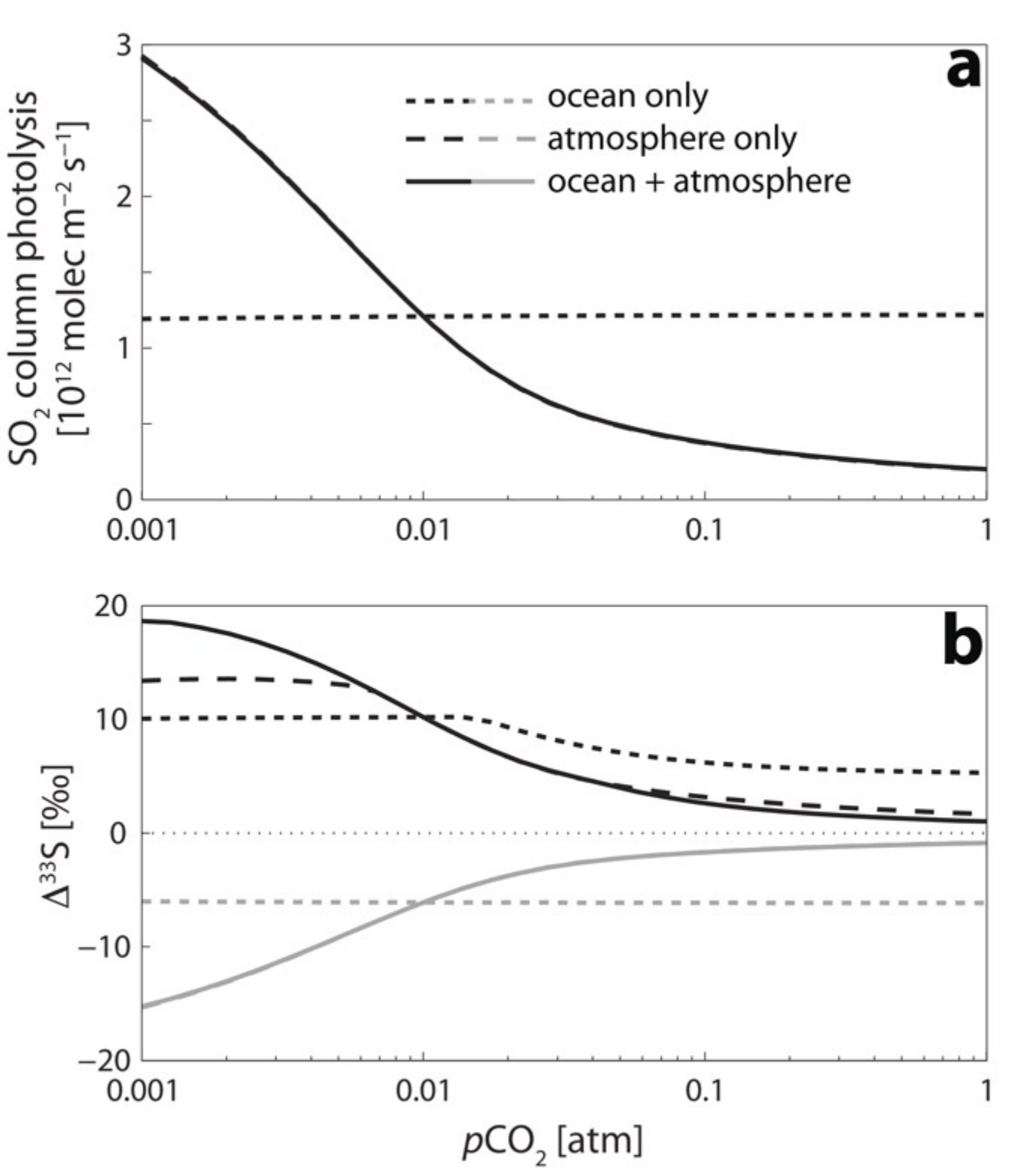
a
ocean only
atmosphere only
ocean + atmosphere
SO2 column photolysis
[10^12 molec m^-2 s^-1]
3
2
1
0
0.001
0.01
0.1
1
b
20
10
0
−10
−20
Δ33S [‰]
0.001
0.01
0.1
1
pCO2 [atm]

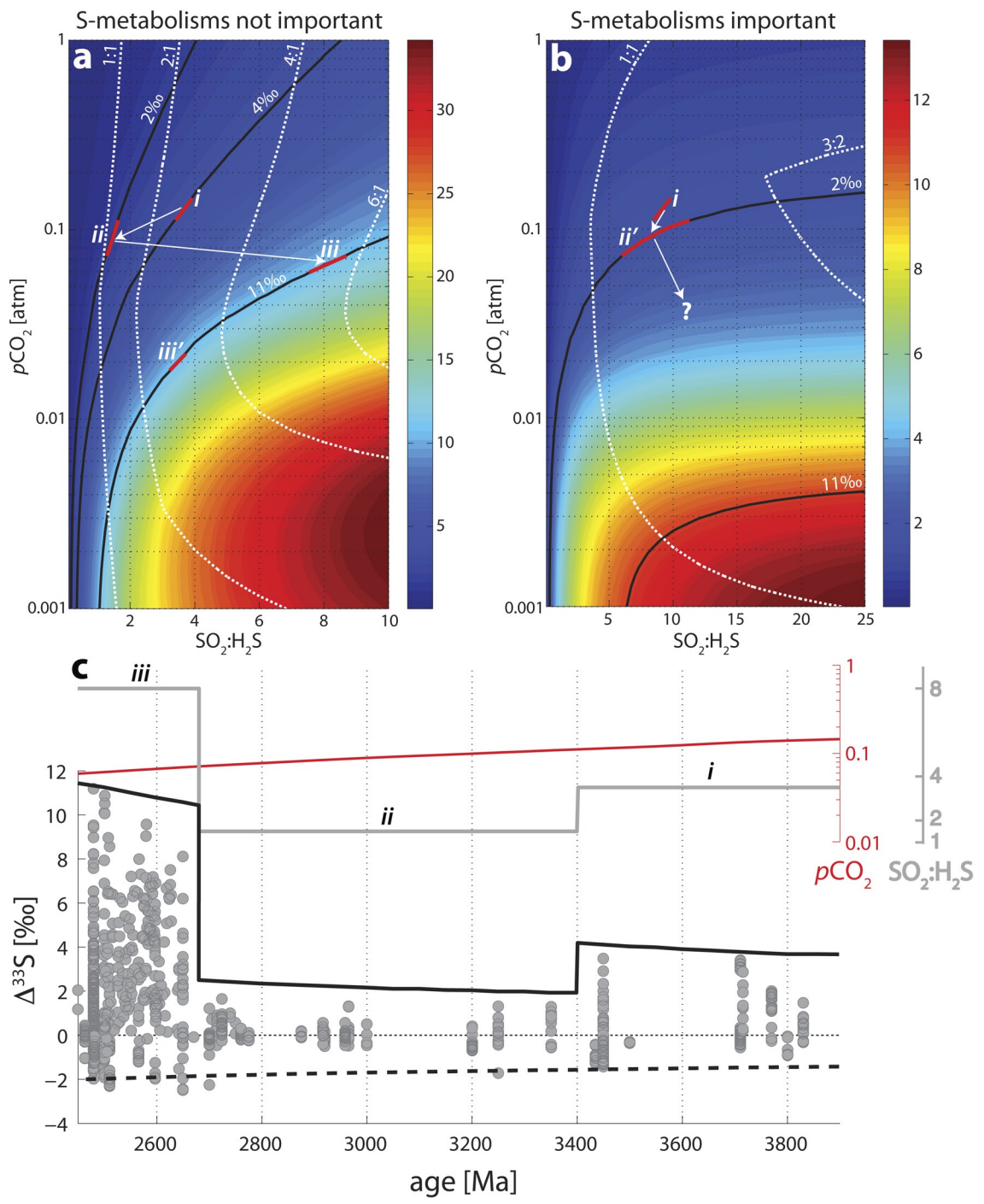
S-metabolisms not important
S-metabolisms important
a
b
c
1:1
2:1
4:1
6:1
2‰
4‰
11‰
3:2
i
ii
ii′
iii
iii′
?
pCO2 [atm]
SO2:H2S
Δ33S [‰]
age [Ma]
pCO2
SO2:H2S